Desalination and Water Treatment
www.deswater.com

doi: 10.5004/dwt.2022.28495

258 (2022) 153–165
May

Textile effluent treatment under artificial and natural irradiation using coupled ZnO-iron ores nanocomposite as photocatalyst

S. Khelifi[a], R. Alsharary[a], Amor Berez[b], L. Mansour[c], A. Choukchou-Braham[d], F. Ayari[a,*]

[a]*Faculty of Sciences of Bizerte, LR 05/ES09 Laboratory of Applications of Chemistry to Resources and Natural Substances and to the Environment (LACReSNE), Carthage University, Zarzouna 7021, Tunisia, emails: fadhilaayari@yahoo.fr (F. Ayari), selma.khelifi@gmail.com (S. Khelifi), reemalsharary@yahoo.fr (R. Alsharary)*
[b]*Laboratoire d'Hydrologie et de Géochimie de Strasbourg (LHyGeS) - UMR 7517 Centre National de Recherche Scientifique, Université de Strasbourg, 1 rue Blessig, 67084 Strasbourg Cedex, France, email: berzamor@yahoo.fr*
[c]*Zoology Department, College of Science, King Saud University, Riyadh, email: lmansour@ksu.edu.sa*
[d]*Université de Tlemcen, Laboratoire de Catalyse et Synthèse en Chimie Organique (LCSCO), Tlemcen 13000, Algeria, email: cba_dz@yahoo.fr*

Received 25 October 2021; Accepted 9 April 2022

ABSTRACT

In this work, we have reported the green synthesis of ZnO nanoparticle and coupled ZnO-iron oxide nanocomposite by sol–gel method using a local iron-ores (labelled TIO: Tamra iron oxide) as iron oxide origin collected from the Tamra deposit (Tunisia). Investigated photocatalysts were tested in the treatment of real textile dyeing effluent. The effluent presents a dark blue color, with a maximum absorbance peak at 594 nm, alkaline pH (pH = 12.4) and high organic contents chemical oxygen demand (COD = 1,400 mg L^{-1}). Experiments were conducted on a lab-scale prototype using UV lamp as artificial light source and solar irradiation as natural light source. The chemical composition and the morphology of the investigated nanocomposites were characterized by X-ray diffraction, scanning electron microscopy, energy-dispersive X-ray spectroscopy and nitrogen adsorption–desorption isotherms. ZnO-iron oxide nanocomposite shows much higher photocatalytic performance with 95% and 91% of color and COD removal within 2 h of UV light irradiation than iron oxide and ZnO nanocomposite. Under solar irradiation, all photocatalysts present high activity for effluent photodegradation compared to UV irradiation and coupled semiconductor ZnO-iron oxide achieves 98.6% and 92% of color and COD removal, respectively in the presence of H_2O_2. Kinetic study was carried out showing that the pseudo-first-order kinetic describes the effluent photodegradation under both irradiation. Characteristics of wastewater after treatment, COD below 250 mg L^{-1}, pH 8.5 and uncolored, respect the condition for releasing in public sewage systems. Experimental findings obtained in this study indicate that ZnO-iron oxide photocatalyst has a great potential application for resolving environmental problems.

Keywords: Photocatalysis; Textile effluent; ZnO nanoparticle; Natural iron-ores; Chemical oxygen demand removal; Coupled semiconductor

1. Introduction

The impact of manufacturing in the textile industry on the environment is considered unsafe at a high level [1]. Like all industries, for the textile one, the imperative is always: produce more, faster, and at a lower cost [1]. The dyeing textile industry remains one of the most polluting. Hence, it is responsible for 17%–20% of water pollution in the world [2]. In addition, a huge amount of water is consumed during the production of the textile [3]. Therefore,

* Corresponding author.

each step of the textile finishing process requires excessive use of pure water followed by a release of wastewater charged of toxic products [4,5]. Discharged effluents are slighted into rivers and lakes creating water pollution and affect the ecosystem [6]. Many dyes from different types are used in a single dyeing operation and a large percentage of the synthetic dye does not bind and is lost in the waste stream [7]. As it has been estimated about 1%–20% of the global production of dyes is released in the textile effluent at the time of dyeing process [7,8].

Due to the reasons mentioned above, wastewater from textile companies is considered as the most polluting by taking into account the composition and the volume of the effluent generated. A wide range of technologies has been developed for the treatment of wastewaters to decrease their environmental impact [9]. In particular, membrane filtration [10], precipitation/coagulation of dyestuffs [11] and chemical methods using traditional oxidants (Cl_2, O_3, …) [12]. Also, adsorption process has been widely employed using various adsorbents such as: activated carbon [13,14] and clay mineral [15]. But these traditional technologies have such disadvantages: the first one is moving simply pollution in large amounts of sludge. The second-one is to be ineffective for certain types of specific dyes. And, finally to be relatively expensive [14,16]. Photocatalysis is a significant advanced oxidation process [17]. It is a useful pre-treatment for hazardous contaminants to enhance their biodegradability. The photocatalytic activity depends on the catalyst ability to create the electron-hole pairs which generate free radicals ($HO^{\bullet}$) which are able to undergo secondary reactions [18]. Besides, the h^+ can directly oxidize organic dyes adsorbed on the surface of catalysts or degrade them indirectly through $HO^{\bullet}$ generated by the reaction between h^+ and water molecules [19].

Among the wide used photocatalysts, TiO_2 and ZnO [19]. ZnO is known in three crystallographic forms: the cubic form (Rocksalt), the blende form and the hexagonal form (wurtzite) [20,21]. The most thermodynamically stable form is the compact hexagonal structure, zincite, with a wurtzite type structure. The properties of ZnO have been known as semiconductor, piezoelectric and active under light irradiation. These characteristics are favorable for photocatalytic reactions [21].

However, the photogenerated electrons are unstable in the excited state, thus can easily recombine to their respective holes. This process dissipates the input light energy and results in low-efficiency photocatalysis [22]. Therefore, the development of a more efficient photocatalyst is an important consideration. Modifications that have been investigated are: altering the textural design, doping and forming composite [23–25]. A composite is a multiphase material that exhibits significant proportion of the properties of all constituent phases such that a better combination of properties is realized [26]. Many researchers have prepared various photocatalysts based on composite and evaluated their photocatalytic performance.

Among them, Fe_2O_3/SiO_2 composite used for methyl orange dye removal [27], $ZnFe_2O_4/ZnO$ composite as photocatalyst for Congo red dye degradation under solar irradiation [25]. Cationic dye degradation was investigated by Fe_2O_3/TiO_2 nanocomposite [26]. In our study in addition to ZnO nanoparticles, we are interested in the natural iron oxide-based composite due to their abundance, availability, and to their physicochemical properties as adsorbent and photocatalyst [28]. Also, in our previous work, this local deposit was evaluated as an adsorbent for azo dye degradation [28]. So, as a continuity of our studies, natural iron oxide was exploited in this work to synthesize ZnO-iron oxide nanocomposite via sol–gel route and the photocatalytic degradation of real textile effluent was investigated.

2. Experimental methodology

2.1. Materials and chemicals

2.1.1. Real textile effluent sampling

The real textile effluent was collected from the unit effluent treatment of a textile industry located in the city of Monastir (East of Tunisia). This company is specialized in yarn manufacturing, indigo dyeing process and textile finishing. The raw effluent was extracted from the effluent input box, situated after the coarse screening. After that, the sample was stored in sealed containers and kept under refrigeration until the moment of use.

2.1.2. Chemicals

Photo-treatment assays of wastewater were performed by means of prepared photocatalysts based on natural iron-oxide doped ZnO nanoparticles. Hydrogen peroxide (32%) and all other chemicals in this work were of analytical grade and used without further purification: zinc chloride hexahydrate ($ZnCl_2{\cdot}6H_2O$), ethanol, and tri-ethanolamine.

2.2. Preparation of the investigated photocatalysts

2.2.1. Natural iron-oxide

The natural mineral used in this study is iron oxide obtained from the deposit of Tamra located in the northeast of the Nefza region (North western of Tunisia). Tamra region contains active iron mines that are very rich in hematite and goethite ores [29]. In addition, this region was described as a mining center in northern Tunisia because of its richness of metals deposits (Fe, Pb, Zn) [29]. Before using this deposit, raw iron oxide sample (reddish brick color) was crushed and sieved and the fraction less than 63 μm was recovered. Homogeneous sample obtained will be noted later in the work by Tamra iron oxide (TIO). The chemical constituents of TIO were found to be Fe_2O_3 (59.76%), CaO (4.87%), SiO_2 (15.38%), Al_2O_3 (5.03%), MnO (2.08%), Cr_2O_3 (0.02%), MgO (0.77%).

2.2.2. Synthesis of ZnO nanoparticle and ZnO-TIO nanocomposite

The investigated photocatalysts were synthesized in this study with simple modification, according to the method explained in the previous work of Hadjltaief et al. [19]. The sol–gel route is described as follows: 4.38 g of zinc chloride were dissolved in 100 mL of ethanol and stirred in a water bath at 50°C. Then, 2.98 g of tri-ethanolamine were

subsequently added to the solution while stirring was continued for 1 h. The mixture was placed under vibration and heated for 30 min at 40°C, conducting to a colourless and transparent sol (ZnO nanoparticles). In the case of iron-oxide (TIO) doped ZnO synthesis, 3 g of TIO were added to this sol. The resulted suspension was agitated under vibration for 30 min, filtered, dried for 12 h, and calcined at 300°C for 4 h. Obtained photocatalysts were labelled ZnO nanoparticle and ZnO-TIO nanocomposite.

2.2.3. Characterization of the photocatalysts

Powder X-ray diffraction (XRD) pattern of the sample was obtained from 2° to 80° range by the diffractometer (PANalytical X'Pert HighScore Plus Diffractometer, Malvern) with monochromatic radiation CuK_{α} (λ = 1.5406 Å). Isotherms of nitrogen adsorption–desorption of materials were measured using Micromeritics Model Triflex (Norcross) surface and porosity analyzer. The specific surface area (S_{BET}) was obtained by the Brunauer–Emmett–Teller (BET) method and the total pore volume (V_p) was calculated at a relative N_2 pressure of P/P_0 = 0.99 at liquid nitrogen temperature of 196°C. Pore size distribution in the mesopore range was calculated using the Barrett–Joyner–Halenda (BJH) method based on the desorption arm of the isotherm. Morphology of the studied materials was investigated by scanning electron microscopy analysis (SEM) with a microscope model Hitachi 3000 (USA). Energy-dispersive X-ray spectroscopy (EDX) coupled to SEM was used to determine the chemical composition of all materials.

2.3. Treatment of real effluent in continuous process

2.3.1. Adsorption experiments

Adsorption tests over the studied photocatalysts were carried out in a batch reactor as follows: a mass of adsorbent (0.2 g) mixed with a 100 mL of textile wastewater, in a 250 mL glass vessel, without pH solution regulation and at room temperature (25°C) under continuous stirring. In order to investigate the effect of contact time, a 3 mL of suspension was sampled at a suitable time interval to measuring the remained effluent concentration in the solution. After the experiment, suspension from each sample was immediately centrifuged and filtered using a 0.45 mm syringe filter.

Adsorption experiments with the studied pollutant were carried out to investigate the adsorption efficiency of the selected photocatalysts and to define the required time of adsorption–desorption equilibrium.

The amount of remaining effluent in the solution was determined by UV-Visible spectrometer (Shimadzu Model Perkin Elmer, Waltham, USA) at maximum absorbance 594 nm. The adsorption percent (% adsorption) was calculated as:

$$\%\ \text{Adsorption} = \frac{C_0 - C_t}{C_0} \times 100 \tag{1}$$

where C_0: initial effluent concentration and C_t: effluent concentration at time t.

2.4. Photochemical treatment of textile effluent

2.4.1. Photoreactor

The photocatalytic treatment of real effluent was carried out in a lab-scale photoreactor irradiated with UV lamp. The photoreactor used is a Pyrex cylinder and its volume is 1 L. A magnetic stirrer was provided to ensure complete homogenization of the solution inside the glass vessel. UV irradiation was provided by a 125 W Philips HPK UV Lamp (UV-A) placed in a plugging tube (Philips, Eindhoven, Netherlands). A Pyrex cylindrical jacket located around the plugging tube allows an irradiation with wavelengths, λ = 350 nm.

2.4.2. Photodegradation tests

All experiments were done at room temperature (T = 25°C) and without pH regulation (natural pH of effluent = 12.4). The photoreactor was filled with 150 mL of effluent. A fixed amount (0.2 g) of photocatalyst was added. Then, the suspension was homogenized during 70 min in the darkness to ensure the adsorption–desorption equilibrium at room temperature. A sample was taken for effluent concentration control, centrifuged and filtered. The lamp was turned ON and the solution was completely exposed to the UV light. Samples were taken at pre-defined times to evaluate the degradation process.

Experiments under natural solar radiation were carried out during the month of May 2020 during sunny days in our laboratory (LCSCO) Tlemcen (Algeria) and were started at 11 am for 2 h.

The decolorization (%) in solution was determined by UV-Vis spectrophotometer (Shimadzu Model Perkin Elmer, Waltham, USA), absorbance measurements were performed at the maximum wavelength of effluent, at 594 nm in natural pH of effluent (12.4). Chemical oxygen demand (COD) concentration was measured by using HACH LANGE DR3900 (Loveland, USA) pH was measured using pH meter HANNA. Before analysis, all samples were centrifuged at 4,000 rpm for 15 min and limpid supernatant liquid were collected and filtered for the determination of COD and absorbance.

The color and COD removals efficiencies were calculated according to Eq. (2):

$$\%\text{RE} = \frac{C_0 - C_t}{C_0} \times 100 \tag{2}$$

3. Results and discussion

3.1. Characterization of raw iron oxide TIO, ZnO and ZnO-TIO photocatalysts

The X-ray diffractograms of natural iron oxide, ZnO nanoparticle and ZnO-TIO nanocomposite are presented in Fig. 2. The XRD patterns of TIO photocatalyst shows that the principal phases constitute this sample are goethite (FeOOH), magnetite (Fe_3O_4) and hematite (Fe_2O_3) confirmed by the presence of their appropriate peaks.

The XRD patterns of ZnO nanoparticles shows strong diffraction peaks at 2θ angles of 32°, 34°, 37°, 47°, 56°, 58°, 63°, 68°, 96°, 72°, and 78° corresponding to the (100), (002),

(101), (102), (110), (103), (200), (112), (201), (004), and (202) reflections of zincite, respectively according to the standardized JCPDS file number 750526 [30]. Well-crystallized diffraction peaks without any characteristic peaks of impurity were observed, suggesting that the ZnO nanoparticle synthesized by our experimental conditions presents high purity and crystallinity. The pattern of ZnO-TIO nanocomposite (Fig. 1), presents the characteristics peaks at 2θ equal to 32°, 34°, 36°, 47°, 55°, and 63° pointing the presence of hexagonal zincite phase of ZnO in this nanocomposite [30]. The characteristics peaks at 26.7°, 34.5°, 36.3° and 41° of 2θ corresponded to (012), (104),(110) and (113) crystal planes of hematite, respectively. The peak at 21.2° of 2θ was due to (110) plane of goethite [28].

A scanning electron microscopy (SEM) was used to characterize the surface morphology of the natural iron oxide, ZnO nanoparticle and ZnO-TIO nanocomposite (Fig. 2A). SEM micrograph of ZnO nanoparticle (Fig. 2Ab) indicates their spherical shape and their white cleaner color. Natural TIO image (Fig. 2Aa) shows spherical to sub-round particles with some agglomeration. Hence, the surface morphology of the nanocomposite ZnO-TIO (Fig. 2Ac and d) clearly shows the change compared to both pure materials.

EDX analysis (Fig. 2B) confirmed the presence of high amount of iron on the surface of natural iron oxide sample, with some amounts of impurities as Si, Ca, Al and Mg. It was further confirmed the purity of ZnO nanoparticle. Also, the nanocomposite ZnO-TIO framework contains both iron and zinc particles.

Textural properties were investigated by nitrogen adsorption–desorption. BET surface area, pore volume, average pore diameter and pore size of the natural iron oxide TIO, ZnO nanoparticle and ZnO-TIO nanocomposite are presented in Table 1. As can be seen, higher values of surface area and porosity were developed by the natural material TIO (48.4 $m^2\ g^{-1}$) compared to the pure ZnO nanoparticle (9.6 $m^2\ g^{-1}$). Hence, the surface area S_{BET} of the nanocomposite was developed to achieve 83.6 $m^2\ g^{-1}$.

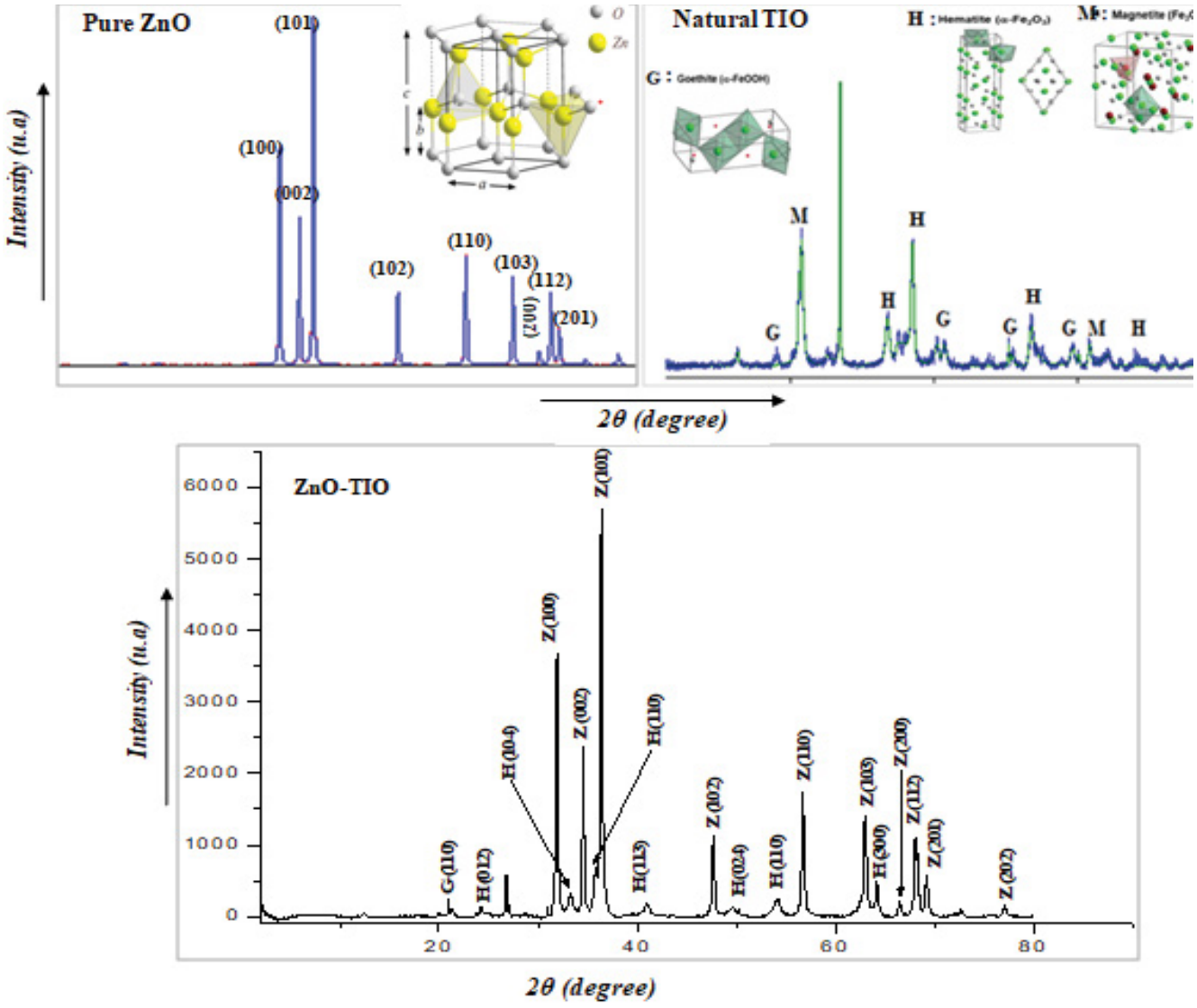

Fig. 1. X-ray diffractograms of the natural TIO, ZnO nanoparticle and ZnO-TIO nanocomposite.

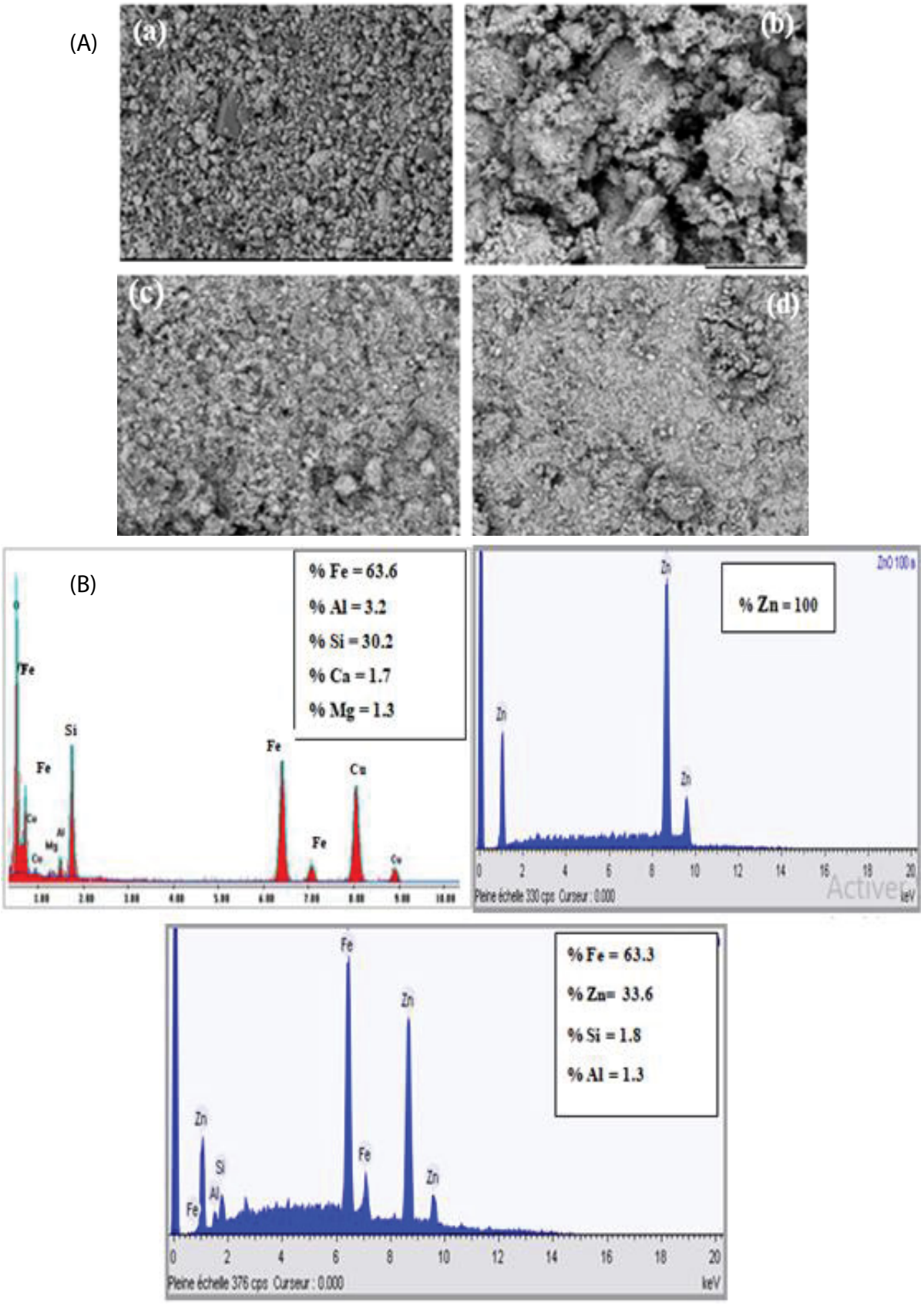

Fig. 2. (A) SEM micrographs of (a) the natural iron oxide TIO, (b) ZnO nanoparticle and (c,d) ZnO-TIO nanocomposite. (B) EDX spectra of the natural iron oxide TIO, ZnO nanoparticle and ZnO-TIO nanocomposite.

The higher values of surface area and porosity of ZnO-TIO nanocomposite can be helpful in the adsorption process by providing better interfacial contact between organic molecules and adsorbent surface. Obtained isotherms (Fig. 3) is a type IV isotherm with a hysteresis loop according to UIPAC classification [31]. Average pore diameter of natural TIO is about 18.9 Å indicating its microporous nature which is enhanced to 41.2 Å after modification by ZnO to form a mesoporous material.

3.2. Effluent characterization

Table 2 presents the main physicochemical characteristics of the effluent sample used in this study. The solution of this wastewater has a dark blue color, a sign of the presence of a significant load of dyes (such as indigo, sulfur dyes, vat dyes) and other chemical products (surfactants, wetting agents, dispersing agents). As can be seen in Table 2, the effluent has an alkaline pH of about 12.4 and therefore

Table 1
Physico-chemical properties of natural TIO, ZnO nanoparticle and ZnO-TIO nanocomposite

Photocatalyst	S_{BET} ($m^2\ g^{-1}$)	S_{BJH}/meso ($m^2\ g^{-1}$)	V_p ($cm^3\ g^{-1}$)	D (Å)	% Fe	% Zn	% Al	% Si
Natural TIO	48.4	44.1	0.18	18.9	63.6	–	3.2	30.2
ZnO	9.6	7.7	0.25	57.40	–	100	–	–
ZnO-TIO	83.6	52.6	0.54	41.2	63.3	33.6	1.8	1.3

S_{BET}: BET surface area; $S_{BJH/meso}$: mesopore surface area; D: average pore diameter; V_p: volume of N_2 adsorbed at $P/P_0 = 0.98$.

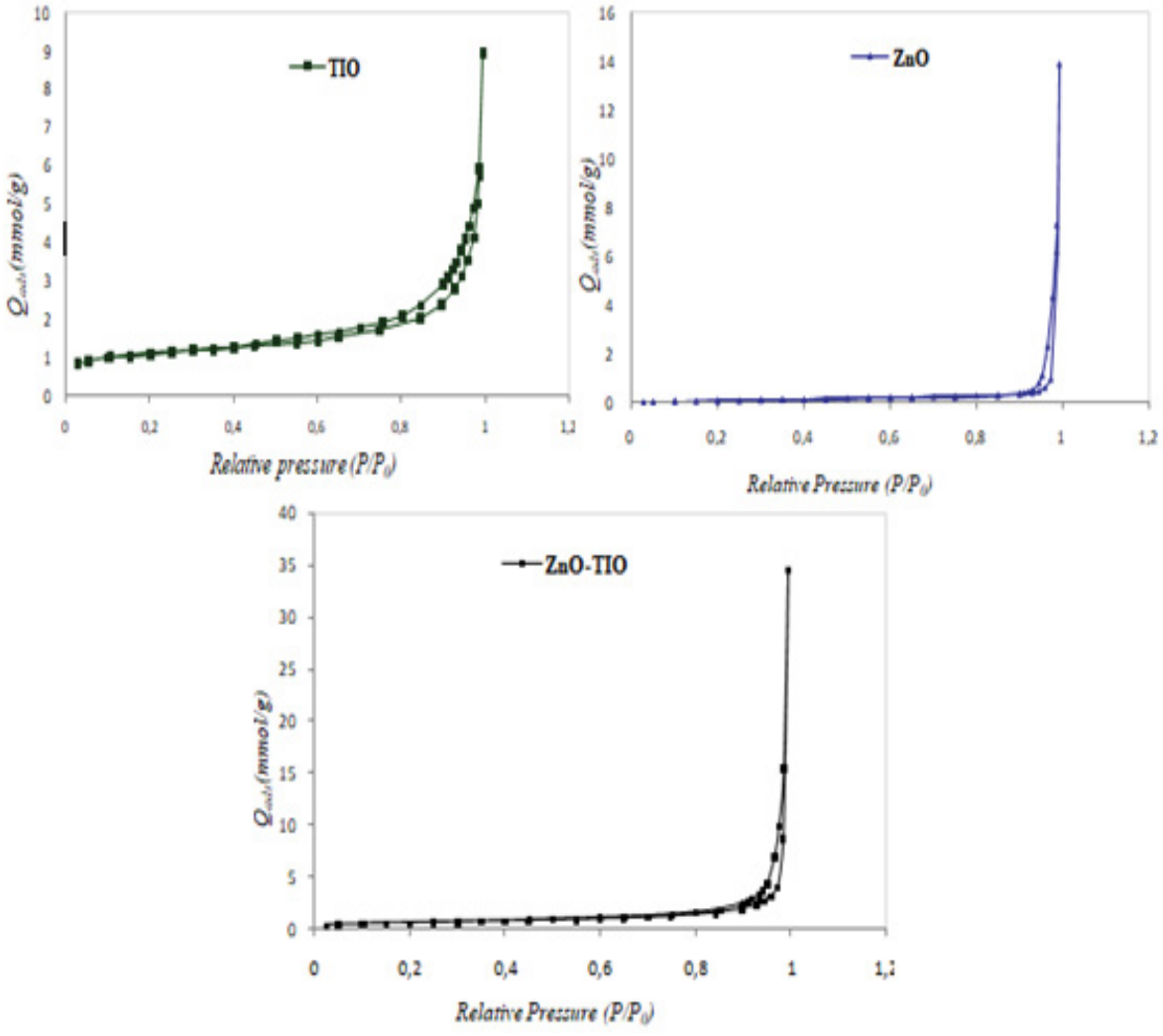

Fig. 3. Adsorption–desorption isotherms of natural TIO, ZnO nanoparticle and ZnO-TIO nanocomposite.

does require neutralization for being acceptable according to Tunisian standards [32]. A conductivity of around 12,372 μS cm^{-1} at 22°C, explains the high presence of ions. Likewise, the effluent has an important value of chemical oxygen demand (COD) which is equal to 1,400 mg L^{-1} and biological oxygen demand (BOD_5) of 400 mg L^{-1}. The values of these two parameters indicate the high level of organic and mineral matter loading. The maximum absorbance peak of this effluent is at 594 nm.

3.3. Adsorption study

Adsorption experiments were conducted in dark conditions, to define the necessary time to reach the adsorption–desorption equilibrium. A fixed amount of photocatalyst (0.2 g) was agitated with 50 mL of effluent for 2 h. 3 mL of suspension were taken at defined times. By centrifugation and filtration, the solid was separated from the liquid phase which was analyzed by spectrophotometer at the maximum absorbance wavelength of the effluent.

As can be seen in Fig. 4, the adsorption percentage for natural iron oxide TIO is about 35% and 43% before and after modification with ZnO, respectively compared to the pure ZnO which is 6%. This is can be explained by the development of the textural properties of the natural material TIO which enhance the adsorptive ability. Also, adsorption–desorption equilibrium was reach around 70 min of adsorbent/adsorbate contact for the three photocatalysts.

Table 2
Textile dyeing effluent characterization

Parameters	Textile wastewater	Tunisian Standards (for river discharge)
pH	12.4	6.5–8.5
MES (mg L^{-1})	200	30
Conductivity (μS cm^{-1})	12,372	1,000
COD (mg L^{-1})	1,400	90
BOD_5 (mg L^{-1})	400	30
Color (Pt-Co)	1,580	70
λ_{max} (nm)	594	–
Cl^- (mg L^{-1})	2,000	600
Oil and grease	10	20
Total hardness	100	5

3.4. Photo-treatment of real effluent

3.4.1. Photodegradation pathway of real effluent under UV irradiation

In order to understand the photodegradation pathway of the studied effluent, many experiments were carried out under different conditions. Fig. 5a illustrates the obtained results in terms of COD and color removals and pH after 2 h of UV irradiation. As can be seen, the photocatalytic activity of the coupled semiconductor ZnO-TIO (77% and 63.9% of COD and color removals, respectively) was higher than the natural material TIO (44% and 28.3% of COD and color removals, respectively), even with ZnO nanoparticle (46% and 25% of COD and color removals, respectively). This is can be explained by the synergetic effect of both particles Zn and iron to photons absorption which confirms their good photocatalytic activity.

The difference in removal efficiency can be explained by the development of surface properties of ZnO-TIO leading to a high adsorption efficiency of textile effluent on the

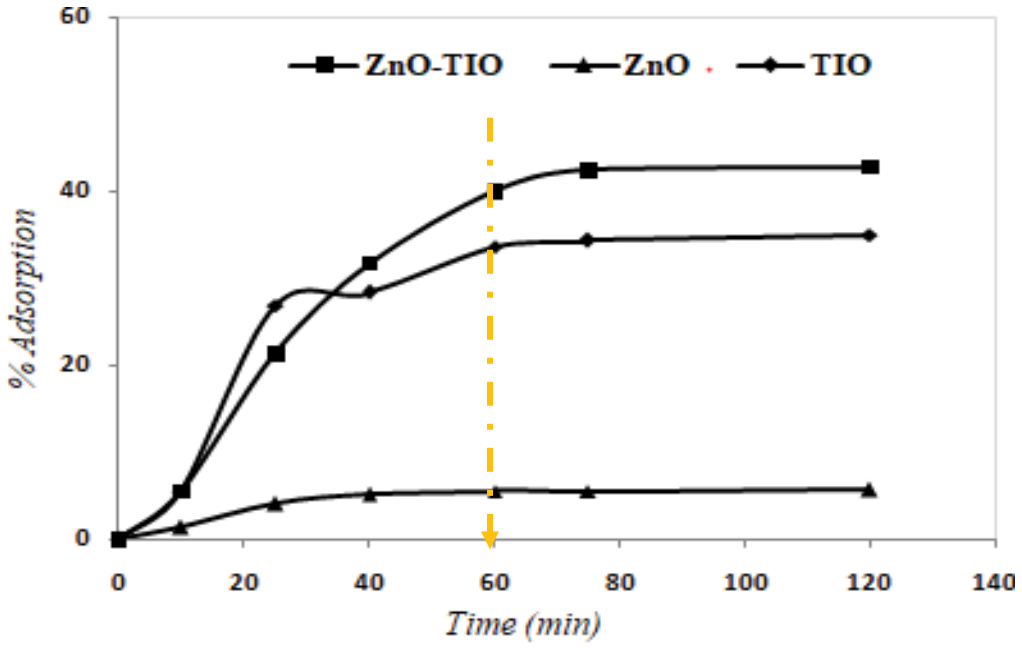

Fig. 4. Kinetics of real effluent adsorption onto natural iron oxide TIO, ZnO nanoparticle and ZnO-TIO nanocomposite (Experimental conditions: 100 mL of effluent; 0.2 g of adsorbent; pH = 12.4; T = 25°C).

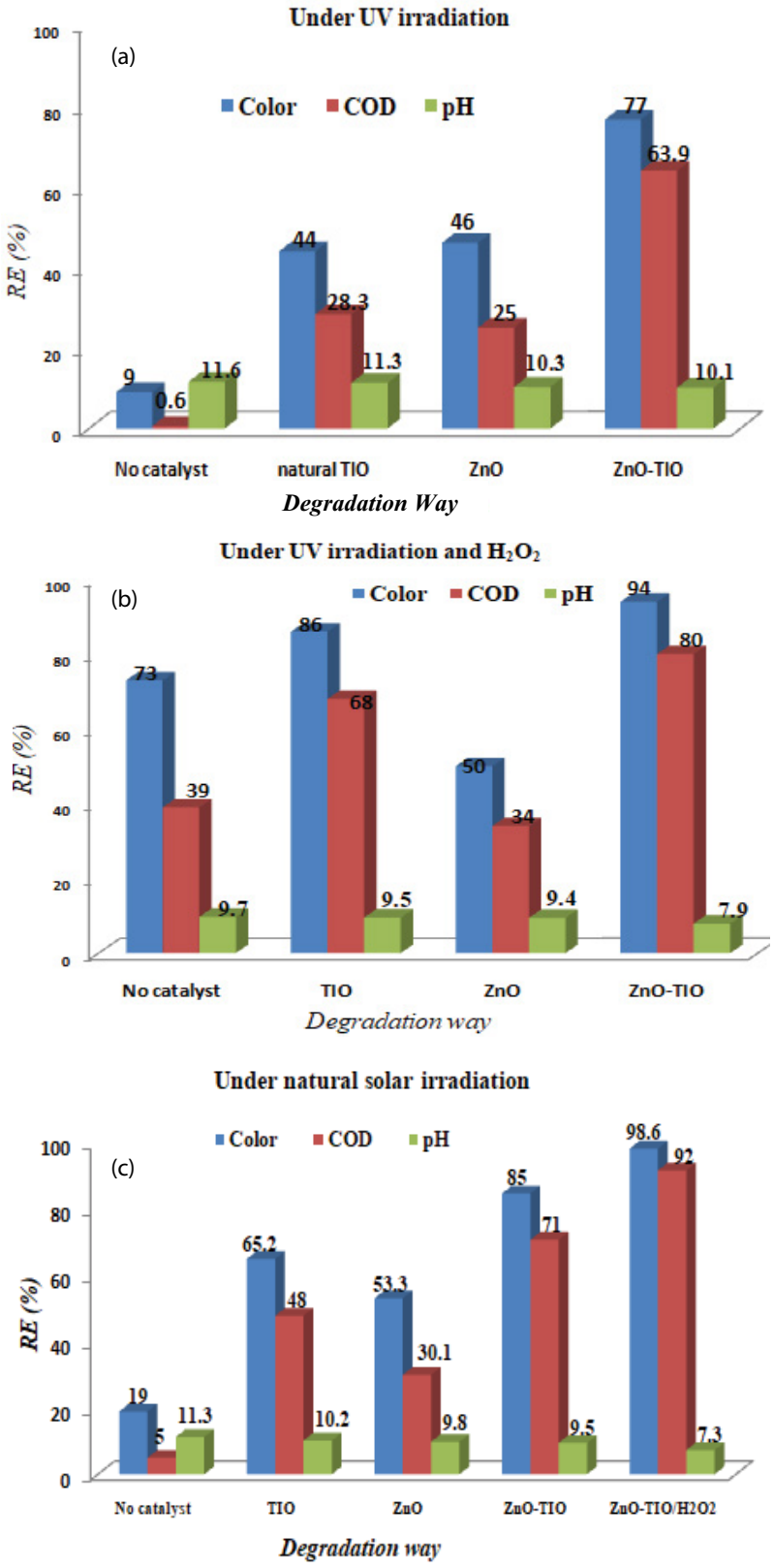

Fig. 5. (a) Removals of color and COD without and with different photocatalysts under UV irradiation (T = 25°C; m_{cata} = 0.2 g; reaction time = 2 h; pH = 12.4). (b) Removals of color and COD without and with different photocatalysts under UV irradiation and in the presence of H_2O_2 (T = 25°C; m_{cata} = 0.2 g; $V_{H_2O_2}$ = 1 mL; reaction time = 2 h; pH = 12.4). (c) Removals of color and COD without and with different photocatalysts under solar irradiation (T = 25°C; m_{cata} = 0.2 g; $V_{H_2O_2}$ = 1 mL; reaction time = 2 h; pH = 12.4).

ZnO-TIO surface (43%). Also, this excellent adsorbability is due to the good activity of natural iron oxide (TIO) as an adsorbent. Most details were reported in our previous work [28] when this material was investigated in the removal of artificial wastewater contains azo dye (Congo red). It is worth noting that photocatalytic processes at semiconductors are based on superficial reactions where adsorption plays an important role [33]. Andreozzi et al. [34] found that the photocatalytic activity of goethite depends strictly on the capability of the substrate to adsorb on the catalyst surface.

In the case of no photocatalyst used, UV irradiation has a negligible effect on the color and COD removals of real effluent.

To enhance the photocatalytic removal of real effluent, photochemical tests were conducted under different conditions including the addition of hydrogen peroxide as oxidant. As can be seen in Fig. 5b, in the case of UV light irradiation combined with H_2O_2 (UV/H_2O_2), colour and COD removals increase to 73% and 39%, respectively because UV light catalysed H_2O_2 to generate the $HO^\bullet$ radicals according to Eq. (3):

$$H_2O_2 + h\nu \rightarrow 2HO^\bullet \quad (3)$$

Also, a greater enhancement in photocatalytic degradation was achieved in the presence of H_2O_2 with the systems (ZnO/UV) (50% and 34% for color and COD removals, respectively) and (TIO/UV) (86% and 68% for color and COD removals, respectively). High removal efficiency was obtained by the mixed semiconductor ZnO-TIO which indicates (94% and 80% for color and COD removals, respectively). This is due to the natural iron oxide TIO which is considered as source of iron who can react with H_2O_2 leading to the formation of supplementary hydroxyl radicals $HO^\bullet$ in the reaction. It is usually called the photo-Fenton reaction.

In summary, the high removal efficiency was resulted by the synergetic effect of different ways as photo-Fenton, H_2O_2 photolysis by UV irradiation and the photocatalytic activity of the studied photocatalyst (ZnO-TIO/UV).

In order to evaluate the contribution of the Fenton process in the photocatalytic oxidation of the real effluent, experiments were done with natural iron oxide TIO as a source of iron and H_2O_2 as an oxidant at room temperature and without pH regulation. Obtained results (Table 3) confirm the contribution of the Fenton reaction in the photocatalytic process. In the dark, natural TIO as a heterogeneous catalyst in Fenton reaction presents 54.6% and 34% of color and COD removal, respectively after 4 h, which is considered an important removal efficiency. H_2O_2 alone has no effect on the real wastewater oxidation (4.5% and 0.03% for color and COD removals, respectively). As can be seen in section 2, the natural TIO presents hematite, goethite, and magnetite as major phases. So, both iron(II) and iron(III) were presented in the framework of the catalyst which enhance the oxidation. Fenton reactions would be described as follows:

$$\equiv Fe(II) - OH + H_2O_2 \rightarrow \equiv Fe(III) + HO^\bullet + HO^- \quad (4)$$

$$\equiv Fe(III) - OH + H_2O_2 \rightarrow \equiv Fe(II) + HO_2^\bullet + H^+ \quad (5)$$

Table 3
Results of Fenton treatment of effluent with both photocatalysts TIO and ZnO-TIO (T = 25°C; m_{cata} = 0.2 g; $V_{H_2O_2}$ = 1 mL; reaction time = 4 h; pH = 12.4)

Process	Color (%)	COD (%)	pH
TIO/H_2O_2	54.6	34	9.5
ZnO-TIO/H_2O_2	52.7	28.4	9.7
H_2O_2 alone	4.5	0.03	10.32

3.4.2. Photodegradation pathway of real effluent under natural solar irradiation

The use of photocatalytic processes under natural solar irradiation for wastewater treatment has a strong performance in a sunny country like North Africa (Tunisia and Algeria) and presents a notably low cost solution. In this section, the removal efficiency of real textile effluent was evaluated under solar irradiation (in Algeria) in the presence of the investigated photocatalysts under same conditions. As seen in Fig. 5c, direct solar photolysis cause a low significant loss of real effluent (19% and 5% for color and COD removals, respectively). In the presence of the studied photocatalysts a notably enhancement in the removal efficiency was noted with the three materials (Fig. 5c) compared with results obtained under UV irradiation. The efficient result was obtained with the addition of H_2O_2 (ZnO-TIO/H_2O_2 system) (98.6% and 92% for color and COD removals, respectively) after 2 h of natural sunlight exposure. Similars results have been reported by Benacherine et al. [35] using sunlight radiation for amoxicillin degradation and in the presence of goethite 25.12% of removal efficiency was obtained after 5 h of natural irradiation compared with 7.1% under UV irradiation.

These results are explained by the fact that solar light covers a broader range of highly energetic ultraviolet and visible radiation [35] able of exciting the photocatalysts (natural iron oxide, ZnO and ZnO-TIO).

3.4.3. Effect of irradiation time and kinetic study

Photocatalytic activity of the coupled semiconductor ZnO-TIO under artificial UV light (125 W) and solar light (in a clear day) for 210 min is shown in Fig. 6. Obtained curves show the remarkable effect of the nature of the used irradiation in the photocatalyst performance. Indeed, the irradiation time has no effect in the removal efficiency. As seen (Fig. 6a), the photocatalytic activity was found to be higher under solar light than under artificial UV light which could be explained by the existence of portion of UV light in the solar spectrum that facilitates the excitation of electron [36].

Photodegradation kinetics is analysed by the defined Langmuir–Hinshelwood (L-H) model [37]. This first-order kinetic model was presented by the following equation:

$$\ln\frac{C_t}{C_0} = -K_{app}t \quad (6)$$

where C_0 and C_t: are the concentrations of effluent at time = 0 and t, respectively, t is the irradiation time and K_{app} is the apparent first-order rate constant (min^{-1}).

By plotting $\ln(C_0/C_t)$ as a function of irradiation time (t) (Fig. 6b), the K_{app} were obtained from the slope of the best fit lines. As shown in Table 4, the photocatalytic reaction obeyed the first-order kinetic according to the correlation coefficient (R^2) and the kinetic constant of ZnO-TIO photocatalyst was found to be higher under solar light than using UV lamp.

3.5. Photodegradation mechanism

It is known that in photocatalytic process using semiconductor, hydroxyl radical can be generated by several ways. The most reported in the literature are summarized as follows:

- Reaction between surface OH groups and iron (in the case of iron oxide semiconductor) as is illustrated in Eq. (7) [35]:

$$\equiv Fe(III) - OH + h\nu \rightarrow \equiv Fe(II) + HO^{\bullet} \quad (7)$$

- Oxidation of H_2O by holes (h^+) formed in the valence band (VB) [38]:

$$ZnO - TIO + h\nu \rightarrow e^- + h^+ \quad (8)$$

$$H_2O + h^+ \rightarrow H^+ + HO^{\bullet} \quad (9)$$

- Reduction of O_2 by electrons photogenerated on semiconductor surface via the conduction band (CB) leading to the formation of $O_2^{\bullet-}$ radicals then $HO^{\bullet}$ radicals, acting as it is reported in reactions sequences [Eqs. (10)–(14)] [38]:

$$O_2 + e^- \rightarrow O_2^{\bullet-} \quad (10)$$

$$O_2^{\bullet-} + H^+ \rightarrow HO_2^{\bullet} \quad (11)$$

$$2HO_2^{\bullet} \rightarrow H_2O_2 + O_2 \quad (12)$$

$$e^-_{(cb)} + O_2^{\bullet-} + 2H^+ \rightarrow H_2O_2 \quad (13)$$

$$e^-_{(cb)} + H_2O_2 \rightarrow OH^- + HO^{\bullet} \quad (14)$$

As it is cited in the literature, that the efficiency of the photocatalysts is related to the separation of the e^-/h^+ pairs.

Table 4
The apparent kinetic constants of the photodegradation reactions of real effluent on ZnO-TIO under artificial UV light and natural solar light

	$K_{app} \times 10^{-3}$ (min^{-1})	R^2
UV	12	0.972
Solar	19	0.98

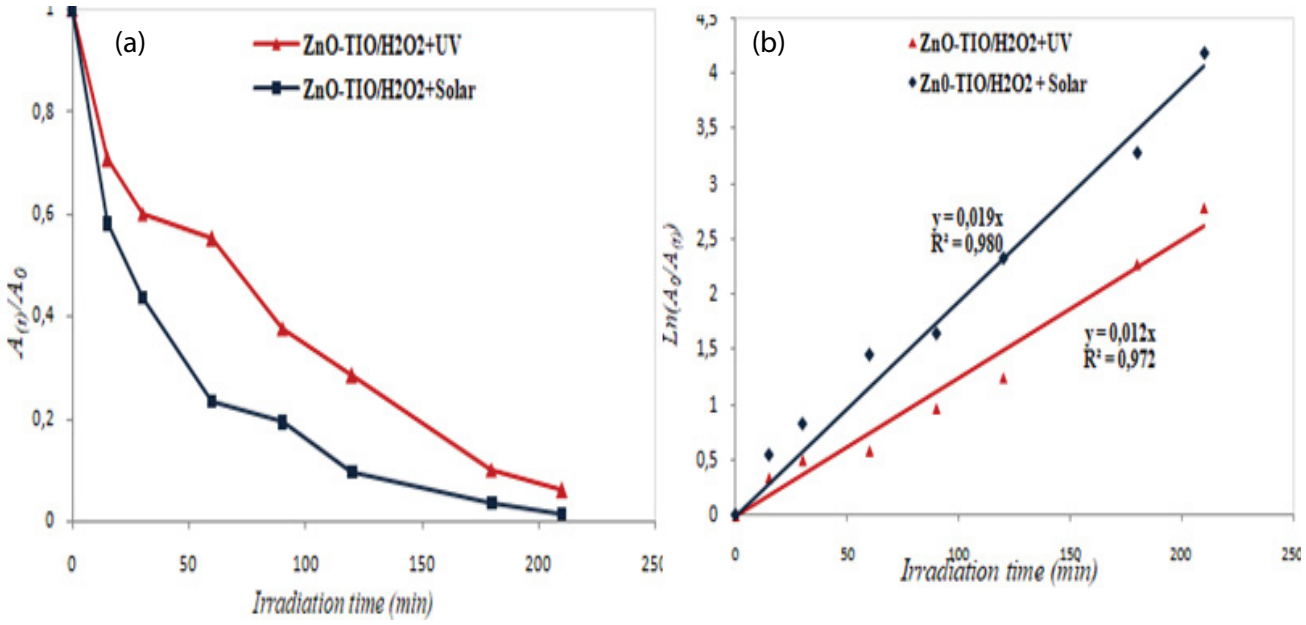

Fig. 6. (a) Relative optical absorbance and (b) $\ln(A_0/A_t)$ for textile effluent photodegradation with ZnO-TIO as function of UV and solar irradiation time.

These latter are menaced by the recombination reactions rather than reacting with the surface species. Therefore, in order to increase the efficiency of the photocatalysts the separation and the amount of the photogenerated e^-/h^+ pairs should be increased.

The mechanism of the charge transfer in the coupled semiconductor ZnO-TIO was proposed as follows: the photoexcited electrons will transfer from the conduction band of ZnO to that of TIO. In the same way, the holes will transfer from the valence band of TIO to the valence band of ZnO. As a result, the electron will remain in the conduction band of TIO and the holes will be accumulated in the valence band of ZnO. Therefore, the nanocomposites have played a crucial role in the enhancement of the separation efficiency of the e^-/h^+ pairs. This enhancement is due to the creation of the heterojunction between ZnO and TIO nanoparticles. Fig. 7 illustrates the relative band positions and the transfer of the photogenerated e^-/h^+ pairs. Similar results were reported by Hamrouni et al. [36]. In their work, they are interested in the degradation of methyl orange by nanosized coupled ZnO/SnO_2 and they explained the same phenomenon by the heterojunctions in coupled ZnO/SnO_2 photocatalyst.

3.6. Characteristics of treated wastewater

After treatment under natural solar irradiation using ZnO-TIO nanocomposite as photocatalyst, the treated effluent was characterized by determining the physicochemical properties. Obtained results (Table 5) show elimination of 98% of the color. In addition, the COD and BOD_5 removal were achieved 92% and 86.25%, respectively which is considered an efficient result. The alkalinity of the medium was decreased from 12.4 to 8, which is considered an acceptable value for releasing in an aquatic medium according to the norm [32]. The COD value reached (180 mg L^{-1}) obeys the

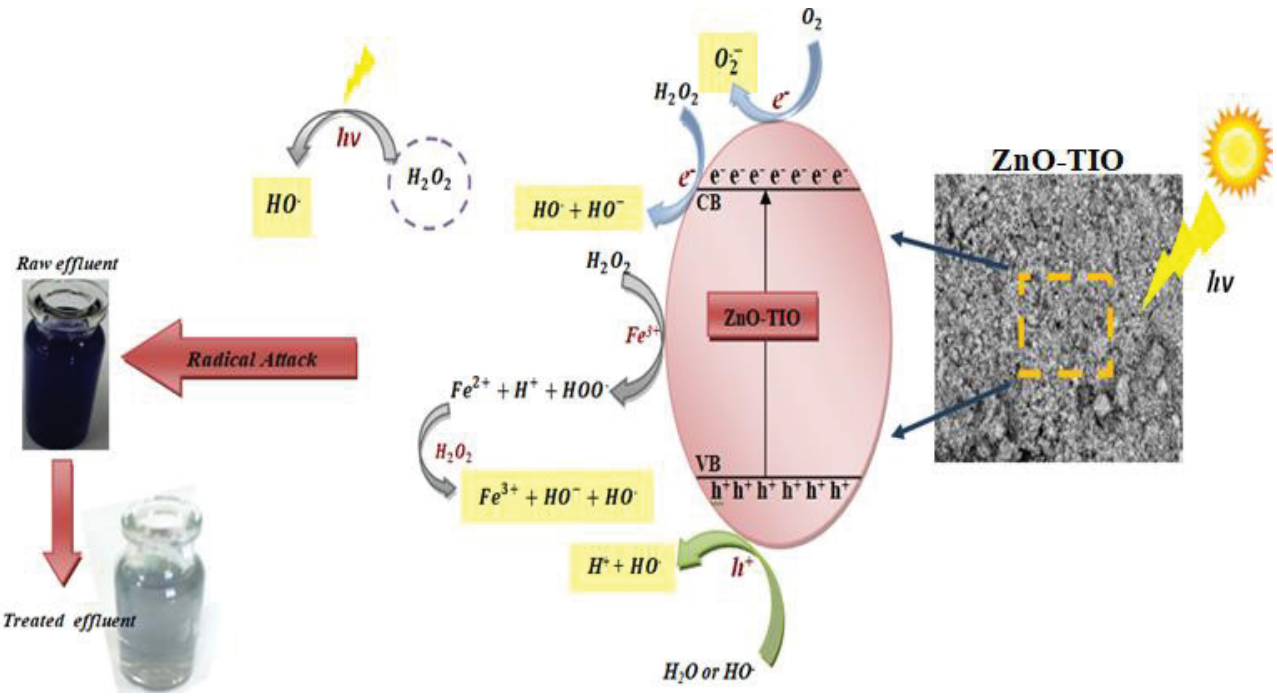

Fig. 7. Mechanism of the photogenerated e^-/h^+ pairs transfer in ZnO-TIO nanocomposite.

Table 5
Most characteristics of real wastewater before and after photocatalytic treatment

Parameters	Before treatment	After treatment	Tunisian Standards (for river discharge)
pH	12.4	8	6.5–8.5
MES (mg L^{-1})	200	10	30
Conductivity (μS cm^{-1})	12,372	3,200	1,000
COD (mg L^{-1})	1,400	180	190
BOD_5 (mg L^{-1})	400	55	60
Colour (Pt-Co)	1,580	65	70
Cl^- (mg L^{-1})	2,000	600	600
Total hardness	100	3	5

Table 6
Comparison of the treatment efficiency with literature studies

Process	Material used	Real effluent	% color removal	% COD removal	Reference
Heterogeneous photocatalysis	Ag-TiO_2	Wastewater effluent	–	80	[17]
Heterogeneous photocatalysis with H_2O_2	TiO_2 (Degussa p25)	Textile printing wastewater	72	58	[39]
Photocatalysis	ZnO-iron oxide (ZnO-TIO)	Textile effluent	98	92	This work
Heterogeneous Fenton process	Zerovalent iron	Textile effluent	70	55	[40]
Adsorption	Purified clay	Textile effluent	–	70	[41]
Homogeneous photo-Fenton	–	Textile wastewater stream	96	20	[42]
Chemical coagulation–electro-oxidation	–	Textile wastewater	100	93%	[43]
Electrocoagulation	–	Textile effluent	90	81	[44]

condition for releasing in public sewage systems. These results confirm the high performance of the prepared photocatalyst based on natural mineral resources.

3.7. Performance comparison with literature data

The efficiency of heterogeneous photocatalysis towards different effluents according to literature data is illustrated in Table 6. Also, the comparison with other processes is highlighted. As can be seen (Table 6), the present work shows an important photocatalytic activity for textile effluent treatment. Consequently, Tunisian materials could be promising photocatalysts for the elimination of pollutants. However, it was evident from the study of photo-treatment of textile wastewater that it would be interesting and it is currently in progress in our laboratory to activate and exploit those materials which can be promising materials for wastewater treatment.

4. Conclusion

In this study, ZnO nanoparticle and ZnO-iron oxide nanocomposite was synthesized via sol–gel route and characterized by means of some techniques. The impact of the investigated materials on textile pollutants was studied by the evaluation of their photocatalytic performance of real textile effluent under UV and solar light irradiations.

In absence of light, the reaction was attributed to the adsorption phenomena and the adsorption–desorption equilibrium was reached after 70 min. In the presence of light, color of the effluent disappears quickly and organics matters were mineralized confirming the high photochemical activity of the studied materials. The coupled ZnO-TIO nanocomposite presents the highest activity compared to pure ZnO and natural TIO. This enhancement is due to the creation of the heterojunctions between ZnO and TIO nanoparticles.

The photodegradation kinetic followed a pseudo-first-order. Under UV irradiation, the effluent degradation reaches 80% in terms of COD removal and 94% in terms of color removal. The use of natural solar irradiation shows more efficient effluent degradation expressed by 98.6% and 92% of color and COD removals, respectively. From the point of view of the practical application in the textile industry as indicated in color and COD removals, photocatalytic degradation using natural resources such as solar irradiation and natural photocatalysts showed the potential to be used as treatment technology.

Acknowledgment

This work was supported by the Research Supporting Project (RSP-2021/75), King Saud University (Riyadh, Saudi Arabia).

References

[1] G. Ghasemzadeh, M. Momenpour, F. Omidi, M.R. Hosseini, M. Ahani, A. Barzegari, Applications of nanomaterials in water treatment and environmental remediation, Front. Environ. Sci. Eng., 8 (2014) 471–482.
[2] F. Ge, H. Ye, M. Li, B.-X. Zhao, Efficient removal of cationic dyes from aqueous solution by polymer-modified magnetic nanoparticles, Chem. Eng. J., 198 (2012) 11–17.
[3] G.B. Patel, P. Rakholiya, T. Shindhal, S. Varjani, N.M. Tabhani, K.R. Shah, Lipolytic *Nocardiopsis* for reduction of pollution load in textile industry effluent and SWISS model for structural study of lipase, Bioresour. Technol., 341 (2021) 125673, doi: 10.1016/j.biortech.2021.125673.
[4] G.C. de Oliveira Neto, P.C. da Silva, H.N.P. Tucci, M. Amorim, Reuse of water and materials as a cleaner production practice in the textile industry contributing to blue economy, J. Cleaner Prod., 305 (2021) 127075, doi: 10.1016/j.jclepro.2021.127075.
[5] P.V. Nidheesh, R. Gandhimathi, S.T. Ramesh, Degradation of dyes from aqueous solution by Fenton processes: a review, Environ. Sci. Pollut. Res., 20 (2013) 2099–2132.
[6] P.K. Majhi, R. Kothari, N.K. Arora, V.C. Pandey, V.V. Tyagi, Impact of pH on pollutional parameters of textile industry wastewater with use of *Chlorella pyrenoidosa* at lab-scale: a green approach, Bull. Environ. Contam. Toxicol., 108 (2022) 485–490.
[7] R. Kishor, D. Purchase, G.D. Saratale, L.F.R. Ferreira, M. Bilal, H.M.N. Iqbal, R.N. Bharagava, Environment friendly degradation and detoxification of Congo red dye and textile industry wastewater by a newly isolated *Bacillus cohnni* (RKS9), Environ. Technol. Innovation, 22 (2021) 101425, doi: 10.1016/j.eti.2021.101425.
[8] M. Wawrzkiewicz, Comparison of the efficiency of Amberlite IRA 478RF for acid, reactive, and direct dyes removal from aqueous media and wastewaters, Ind. Eng. Chem. Res., 51 (2012) 8069–8078.
[9] U. Nimkar, Sustainable chemistry: a solution to the textile industry in a developing world, Curr. Opin. Green Sustainable Chem., 9 (2018)13–17.
[10] Z. Hu, H. Chen, F. Ji, S. Yuan, Removal of Congo red from aqueous solution by cattail root, J. Hazard. Mater., 173 (2010) 292–297.

[11] C. O'Neill, F.R. Hawkes, D.L. Hawkes, N.D. Lourenço, H.M. Pinheiro, W. Delée, Colour in textile effluents – sources, measurement, discharge consents and simulation: a review, J. Chem. Technol. Biotechnol., 74 (1999) 1009–1018.
[12] X.-C. Jin, G.-Q. Liu, Z.-H. Xu, W.-Y. Yao, Decolorization of a dye industry effluent by *Aspergillus fumigatus* XC6, Appl. Microbiol. Biotechnol., 74 (2007) 239–243.
[13] R.C.C. Costa, M.F.F. Lelis, L.C.A. Oliveira, J.D. Fabris, J.D. Ardisson, R.R.V.A. Rios, C.N. Silva, R.M. Lago, Novel active heterogeneous Fenton system based on $Fe_{3-x}M_xO_4$ (Fe, Co, Mn, Ni): the role of M^{2+} species on the reactivity towards H_2O_2 reactions, J. Hazard. Mater., 129 (2006) 171–178.
[14] Z. Deng, S. Sun, H. Li, D. Pan, R.R. Patil, Z. Guo, I. Seok, Modification of coconut shell-based activated carbon and purification of wastewater, Adv. Compos. Hybrid Mater., 4 (2021) 65–73.
[15] O.S. Omer, M.A. Hussein, B.H. Hussein, A. Mgaidi, Adsorption thermodynamics of cationic dyes (methylene blue and crystal violet) to a natural clay mineral from aqueous solution between 293.15 and 323.15 K, Arabian J. Chem., 11 (2018) 615–623.
[16] Z. Antonio, L. Roberto, Evaluation of UV/H_2O_2 advanced oxidation process (AOP) for the degradation of diazo dye Reactive Green 19 in aqueous solution, Desal. Water Treat., 52 (2013) 1571–1577.
[17] H. Chaker, L. Chérif-Aouali, S. Khaoulani, A. Bengueddach, S. Fourmentin, Photocatalytic degradation of methyl orange and real wastewater by silver doped mesoporous TiO_2 catalysts, J. Photochem. Photobiol., A, 318 (2016) 142–149.
[18] R. Tanwar, S. Kumar, U.K. Mandal, Photocatalytic activity of PANI/Fe^0 doped BiOCl under visible light-degradation of Congo red dye, J. Photochem. Photobiol., A, 333 (2017) 105–116.
[19] H.B. Hadjltaief, M. Ben Zina, M.E. Galvez, P. Da Costa, Photocatalytic degradation of methyl green dye in aqueous solution over natural clay-supported ZnO–TiO_2 catalysts, J. Photochem. Photobiol., A, 315 (2016) 25–33.
[20] S.Y. Lee, E.S. Shim, H.S. Kang, S.S. Pang, J.S. Kang, Fabrication of ZnO thin film diode using laser annealing, Thin Solid Films, 437 (2005) 31–34.
[21] M. Guo, W. Jiang, C. Chen, S. Qu, J. Lu, W. Yi, J. Ding, Process optimization of biodiesel production from waste cooking oil by esterification of free fatty acids using La^{3+}/ZnO-TiO_2 photocatalyst, Energy Convers. Manage., 229 (2021) 113745, doi: 10.1016/j.enconman.2020.113745.
[22] N. Roy, S. Chakraborty, ZnO as photocatalyst: an approach to wastewater treatment, Mater. Today: Proc., 46 (2021) 6399–6403.
[23] T.A. Saleh, V.K. Gupta, Photo-catalyzed degradation of hazardous dye methyl orange by use of a composite catalyst consisting of multi-walled carbon nanotubes and titanium dioxide, J. Colloid Interface Sci., 371 (2012) 101–106.
[24] K. Dai, L. Lu, C. Liang, J. Dai, G. Zhu, Z. Liu, Q. Liu, Y. Zhang, Graphene oxide modified ZnO nanorods hybrid with high reusable photocatalytic activity under UV-LED irradiation, Mater. Chem. Phys., 143 (2014) 1410–1416.
[25] A. Ahmad, S.H. Mohd-Setapar, C.S. Chuong, A. Khatoon, W.A. Wani, R. Kumar, M. Rafatullah, Recent advances in new generation dye removal technologies: novel search for approaches to reprocess wastewater, RSC Adv., 5 (2015) 30801–30818.
[26] T. Madrakian, A. Afkhami, R. Haryania, M. Ahmadi, Synthesis of γ-Fe_2O_3/TiO_2 nanocomposite and its application in removal of dyes from water samples by adsorption and degradation processes, RSC Adv., 4 (2014) 44841–44847.
[27] W. Deligeer, Y.W. Gao, S. Asuha, Adsorption of methyl orange on mesoporous Fe_2O_3/SiO_2 nanocomposites, Appl. Surf. Sci., 257 (2011) 3524–3528.
[28] S. Khelifi, A. Choukchou-Braham, M.H. Oueslati, H.M. Sbihi, F. Ayari, Identification and use of local iron-ores deposit as adsorbent: adsorption study and photochemical regeneration, Desal. Water Treat., 206 (2020) 429–438.
[29] S. Decrée, C. Marignac, T. De Putter, E. Deloule, J.-P. Liégeois, D. Demaiffe, Pb–Zn mineralization in a Miocene regional extensional context: the case of the Sidi Driss and the Douahria ore deposits (Nefza mining district, northern Tunisia), Ore Geol. Rev., 34 (2008) 285–303.
[30] H. Xu, D. Zhang, A. Xu, F. Wu, R. Cao, Quantum sized zinc oxide immobilized on bentonite clay and degradation of C.I. Acid red 35 in aqueous under ultraviolet light, Int. J. Photoenergy, 2015 (2015) 7–17.
[31] K.S.W. Sing, Reporting physisorption data for gas/solid systems with special reference to the determination of surface area and porosity (Provisional), Pure Appl. Chem., 54 (1982) 2201–2218.
[32] NT 106.02 TS-BoJbtMotNE, Implementing the Tunisian Standard Concerning Wastewater Effluent Discharges in the Hydrous Medium, 1989, p. 1332.
[33] J. Rashid, M.A. Barakat, Y. Ruzmanova, A. Chianese, Fe_3O_4/SiO_2/TiO_2 nanoparticles for photocatalytic degradation of 2-chlorophenol in simulated wastewater, Environ. Sci. Pollut. Res., 22 (2015) 3149–3157.
[34] R. Andreozzi, V. Caprio, R. Marotta, Iron(III) (hydr)oxide-mediated photooxidation of 2-aminophenol in aqueous solution: a kinetic study, Water Res., 37 (2003) 3682–3688.
[35] M. El Mehdi Benacherine, N. Debbache, I. Ghoul, Y. Mameri, Heterogeneous photoinduced degradation of amoxicillin by goethite under artificial and natural irradiation, J. Photochem. Photobiol., A, 335 (2017) 70–77.
[36] A. Hamrouni, H. Lachheb, A. Houas, Synthesis, characterization and photocatalytic activity of ZnO-SnO_2 nanocomposites, Mater. Sci. Eng., B, 178 (2013) 1371–1379.
[37] C.H. Nguyen, H.N. Tran, C.-C. Fu, Y.-T. Lu, R.-S. Juang, Roles of adsorption and photocatalysis in removing organic pollutants from water by activated carbon–supported titania composites: kinetic aspects, J. Taiwan Inst. Chem. Eng., 109 (2020) 51–61.
[38] H.B. Hadjltaief, S.B. Ameur, P. Da Costa, M. Ben Zina, M.E. Galvez, Photocatalytic decolorization of cationic and anionic dyes over ZnO nanoparticle immobilized on natural Tunisian clay, Appl. Clay Sci., 152 (2018) 148–157.
[39] M. Iqbal, M.Z. Ahmad, I.A. Bhatti, K. Qureshi, A. Khan, Cytotoxicity reduction of wastewater treated by advanced oxidation process, Chem. Int., 1 (2015) 53–59.
[40] Y. Segura, F. Martínez, J.A. Melero, J.L.G. Fierro, Zerovalent iron (ZVI) mediated Fenton degradation of industrial wastewater: treatment performance and characterization of final composites, Chem. Eng. J., 269 (2015) 298–305.
[41] F. Ayari, S. Khelifi, M. Trabelsi-Ayadi, Synthesized and characterization of organobentonites for anionic dye removal: application to real textile effluent, Environ. Technol., 40 (2019) 2986–3002.
[42] S.F. Kang, C.H. Liao, S.T. Po, Decolorization of textile wastewater by photo Fenton oxidation technology, Chemosphere, 41 (2000) 1287–1294.
[43] E. GilPavas, I. Dobrosz-Gómez, M.Á. Gómez-García, Optimization of sequential chemical coagulation–electro-oxidation process for the treatment of an industrial textile wastewater, J. Water Process Eng., 22 (2018) 73–79.
[44] O. Tünay, M. Simşeker, I. Kabdaşli, T. Olmez-Hanci, Abatements of reduced sulphur compounds, colour, and organic matter from indigo dyeing effluents by electrocoagulation, Environ. Technol., 35 (2014) 1577–1588.